Mechanism of mass transfer of indicator ions to an oxygen-evolving and a hydrogen-evolving electrode in alkaline solution

Electrochimica Acta, Vol. 30, No. 5, pp. 683–694, 1985.
Printed in Great Britain.

0013–4686/85 $3.00 + 0.00

MECHANISM OF MASS TRANSFER OF INDICATOR IONS TO AN OXYGEN-EVOLVING AND A HYDROGEN-EVOLVING ELECTRODE IN ALKALINE SOLUTION

L. J. J. JANSSEN and E. BARENDRECHT

Laboratory for Electrochemistry, Department of Chemistry, Eindhoven University of Technology, P.O. Box 516, 5600 MB Eindhoven, The Netherlands

(*Received* 11 *July* 1984; *in revised form* 4 *October* 1984)

Abstract—A new convection-penetration model for mass transfer of indicator ions to a gas-evolving electrode at forced convection of solution is described theoretically. To check this model, the mass transfer coefficients for ferricyanide ions and ferrocyanide ions to, respectively, a hydrogen-evolving and an oxygen-evolving electrode in 1 M KOH and at 298 K and various bulk-solution flow velocities have been determined in the usual way. The average diameter, cross-section and volume of detached bubbles and the efficiency of gas bubble evolution, have been determined photographically, however. It has been found that the mass transfer of indicator ions to a gas-evolving electrode can be described well by the new model. The contribution of an oxygen bubble departing from the electrode surface to the mass transfer is much greater than the contribution of a departing hydrogen bubble.

NOMENCLATURE

a_d	proportional factor
A_d	average cross-section of detached bubbles; bubble cross-section (m^2)
A_e	surface area of electrode (m^2)
c_i	concentration of species i in bulk of solution ($mol\,m^{-3}$)
d	bubble density of sites from which bubbles depart (m^{-2})
D_i	diffusion coefficient of species i ($m^2\,s^{-1}$)
E	electrode potential *vs sce* (V)
F	$= 96{,}487 \times 10^6\,C\,kmol^{-1}$, Faraday constant
h_{RS}	slope of $\log R_{S,d}/\log i$ curve
i	electric current density ($kA\,m^{-2}$)
I	electric current (kA)
k_i	mass transfer coefficient of the indicator ion i ($m\,s^{-1}$)
k_i^0	mass transfer coefficient of the indicator ion i in absence of forced convection or in a convectionless solution ($m\,s^{-1}$)
$k_{e,i}$	mass transfer coefficient of the indicator ion i obtained by extrapolation of k_i/i curve ($m\,s^{-1}$)
$k_{f,i}$	mass transfer coefficient of the indicator ion i at forced convection in absence of gas bubble evolution ($m\,s^{-1}$)
k_i'	mass transfer coefficient of the indicator ion i in convectionless conditions for the part of electrode surface from which a bubble had departed ($m\,s^{-1}$)
$k_{i,a}'$	average value of k_i' for period t_d ($m\,s^{-1}$)
$k_{f,i}'$	mass transfer coefficient of the indicator ion i at forced convection for the part of electrode surface from which a bubble had departed ($m\,s^{-1}$)
$k_{f,i,a}'$	average value of $k_{f,i}'$ for period t_1 ($m\,s^{-1}$)
$k_{f,i,a*}'$	average value of $k_{f,i}'$ for period t_d ($m\,s^{-1}$)
m_i	mass flux density of the indicator ion i ($mol\,m^{-2}\,s^{-1}$)
N	number of detached bubbles per unit surface area and time ($cm^{-2}\,s^{-1}$)
n	number of bubbles on a picture or on a part of a moving film (1)
n	number of electrons, involved in the reaction to form one molecule of a species (1)
p	a proportional factor
R_d	average radius of departed bubbles; bubble radius (m)
$R_{d,i}$	radius of the departed bubble i (m)
$R_{d,m}$	maximum radius of departed bubble (m)
$R_{S,d}$	Sauter bubble radius; $R_{S,d} = 3V_d/4A_d$ (m)
s	fraction of electrode surface coming into contact with fresh bulk electrolyte in period t_d (1)
t	time (s)
t_d	bubble cycle time (s)
t_1	time $D_i/\pi k_{f,i}^2$ (s)
T	temperature (K)
v_b	absolute rising velocity of bubble ($m\,s^{-1}$)
v_g	volumetric gas production rate ($m\,s^{-1}$)
$v_{g,b}$	volumetric production rate of gas bubbles ($m\,s^{-1}$)
v_g'	volumetric production rate of gas bubbles when all the gas is evolved as bubbles ($m\,s^{-1}$)
v_s	solution flow velocity ($m\,s^{-1}$)
v_d	average volume of departed bubbles; bubble volume (m^3)
V_M	volume of 1 mol gas; $24.4 \times 10^{-3}\,m^3$ at 298 K ($m^3\,mol^{-1}$)
η_g	efficiency of gas bubble evolution (%)

Subscripts

a	average value
b	bubbles
d	detached bubble
e	electrode; extrapolated
f	forced convection
fi	ferricyanide ion
fo	ferrocyanide ion
g	gas
H	hydrogen
i	indicator ion i
m	maximum
O	oxygen
s	solution

1. INTRODUCTION

Mass transfer at gas-evolving electrodes has been studied extensively over the last twenty years because

of its great importance in various industrial processes, *eg* chlorine, aluminium and zinc electrolysis. In particular, the mass transfer of indicator ions to a gas-evolving electrode at natural convection has been thoroughly investigated and various mass transfer models are available[1–6].

Up till now, a model describing the mass transfer of indicator ions to a gas-evolving electrode at forced convection of bulk solution has not been presented in the literature. However, some empirical correlations[7, 8] to calculate the mass transfer coefficient k for a gas-evolving electrode at forced convection of bulk solution are given. The simplest correlation has been proposed by Beck[7], *viz.*

$$k = k_f + k^0$$

where k_f is the mass transfer coefficient for hydrodynamic flow without the presence of bubbles; k^0 is the mass transfer coefficient for a gas-evolving electrode under natural convection conditions.

The main purpose of this study is to elucidate a model for the mass transfer of indicator ions to a gas-evolving electrode with superposition of hydrodynamic flow of solution. The proposed model is a modification of the coalescence model given by Janssen and van Stralen[4]. To check the modified model, it is necessary to determine some parameters characterizing detaching bubbles, and to determine the fraction of the gas formed which departs from the electrode surface in the form of bubbles. This fraction is called the efficiency of gas evolution[9].

So far, no experimental data on the efficiency of gas evolution are available and only some calculated results have been reported[9].

2. EXPERIMENTAL

2.1. *Determination of parameters of detached bubbles and efficiency of gas evolution*

2.1.1. *Electrolytic cell and circuit.* The electrolytic cell used in the optical experiments is sketched in Fig. 1. The working-electrode compartment and the two counter-electrode compartments are separated by porous glass diaphragms. The main part of the working-electrode compartment consists of a square tub with an inner cross-section of $10 \times 10\,mm^2$ and a length of about 100 mm.

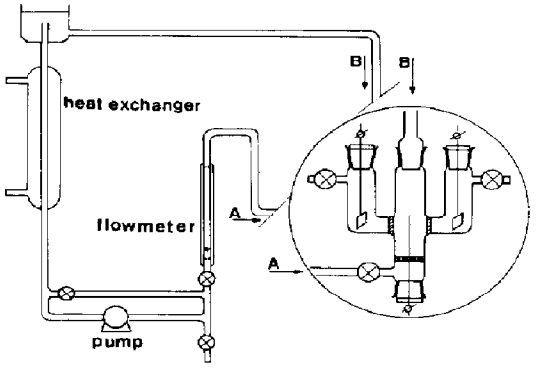

Fig. 1. Schematic diagram of electrolytic cell and solution circuit for optical experiments.

The thermostatted solution was pumped through the working-electrode compartment; its volumetric flow rate was measured with a calibrated flowmeter (Fischer and Porter Tube: 3 F-3/8-25-5, Float CD-38, float material: glass density 2.28 $g\,cm^{-3}$). This solution was saturated with oxygen or hydrogen, respectively, when oxygen or hydrogen experiments were carried out.

Special care was taken to prevent the presence of gas bubbles in the solution at the entrance of the working-electrode compartment. The temperature of the solution in the working-electrode compartment was kept on 298 K. To prevent solution-flow instabilities and obtain a parallel solution flow, a grid was placed in the lowest part of the cell. Gas evolved at the counter electrodes left the cell *via* special valves.

The working electrode was a nickel wire 0.5 mm in diameter and 5.45 mm in length. This electrode was placed vertically in the middle of the tub opposite the glass diaphragms. Two platinum plates $30\,mm^2$ each were used as the counter electrodes. The current has been adjusted galvanostatically. A 1 M KOH solution was used as electrolyte for all experiments.

After a pre-electrolysis of 1.5 h at the highest current in the series of experiments, experiments were carried out at decreasing current density. Four different solution-flow velocities, *viz.* 0.12, 0.09, 0.06 and 0.04 $m\,s^{-1}$ were used for oxygen evolution and only one, *ie* 0.12 $m\,s^{-1}$ for hydrogen evolution.

2.1.2. *Optical measurements.* Against-the-light photography has been used to show the hydrogen and oxygen bubbles just above the working electrode. The experimental set-up used is practically the same as described in the literature[10, 16].

The bubbles were pictured by either photographs or moving films. The photographs were taken with a still camera. In this case a nanolite flashlight with a flash time of approximately 20 ns was used to take sharp pictures of the moving bubbles.

The film was taken with a high-speed film camera (Hitachi, type NAC 16D) with a picture frequency of 3000 frames per second to obtain sharply pictured bubbles.

Bubbles moving through a region, the lower edge of which is situated about 1 mm above the top of the test electrode, were pictured in all optical experiments.

No bubbles rose outside the pictured region, which is 0.71 mm in width and 0.47 mm in height for the film. For the photograph the width is 1.46 mm and the height 0.97 mm. Moreover, the depth of sharpness of the pictured region was sufficient to picture all the bubbles present in this region sharply. The photographs and the single films were analyzed as described in the literature[10, 16].

The high-speed films showed that the velocity of pictured bubbles was not equal to that of the flow of the bulk solution. Consequently, the single photograph experiments are not useful in determining the efficiency of gas evolution.

To obtain the volumetric rate of gas-bubble evolution, the diameter of each bubble moving across a fixed straight on the film pictures, taken during a fixed time, was measured.

The measured bubbles in these pictures, about 100 to 200, were also used to determine the bubble parameters. These parameters were also obtained from the bubbles shown on five photographs. In this case the diameter of about 30 bubbles was measured.

2.2. *Determination of rate of mass transfer at forced convection*

2.2.1. *Electrolytic cell and electrolyte circuits.* The electrolytic cell used for all mass transfer experiments is a two-compartment acrylate cell, the compartments being separated by an ion-exchange membrane (Nafion, type 427). Parts of the electrolytic cell are schematically shown in Fig. 2. The inner dimensions of both compartments are the same: height 100 mm, width 30 mm and depth, the distance from the membrane to the inner back-wall of the rectangular compartment, 10 mm. In each compartment the solution inlet and outlet are at the bottom and top, respectively. An acrylate support of the working electrode was placed in the working-electrode compartment, so that the cross-section of solution flow at the level of the working electrode was 100 mm^2 and the distance from the working electrode to the membrane 7.5 mm. The working electrode was 8.0 mm in width and 60 mm in height; it was insulated at the rear. The counter electrode, made of Veco gauze, had the same geometrical dimensions and was pressed against the membrane just opposite the working electrode.

Solution circuits similar to the one schematically represented in Fig. 1 were used for both compartments of the cell. The size of the solution reservoir was sufficient to allow all bubbles to escape from the circulating solution. For bulk-solution-flow velocities higher than 0.12 $m\,s^{-1}$ the CD-38 float was replaced by a SS-38 float of stainless steel with a density of 8.02 $g\,cm^{-3}$.

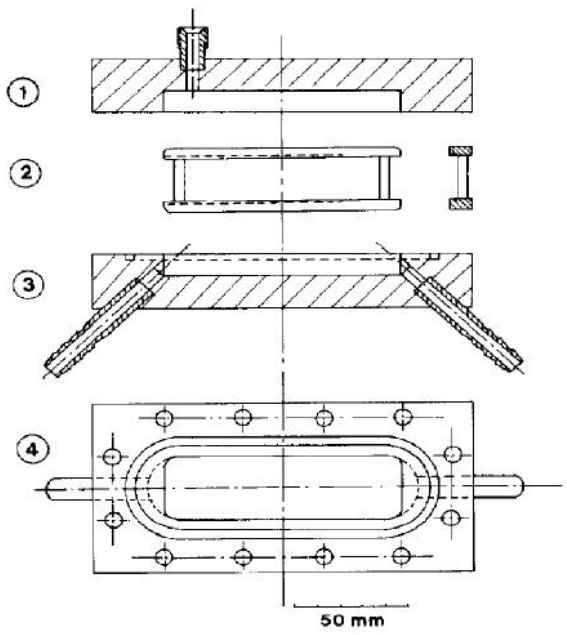

Fig. 2. Schematic diagramof electrolytic cell for mass transfer experiments. 1, Cross-section A–B of working electrode compartment. 2, Top view of electrode support. 3, Cross-section A–B of counter electrode compartment. 4, Top view of counter electrode compartment.

2.2.2. *Electrolyte, analysis and procedure.* A 1 M KOH solution was used as supporting electrolyte for all experiments. To determine the mass transfer coefficients for the oxygen-evolving electrode and the hydrogen-evolving electrode, respectively, $K_4Fe(CN)_6$ and $K_3Fe(CN)_6$, were added to the supporting electrolyte[11]. At the beginning of a series of experiments the concentration of the indicator ion was about 0.05 M, unless otherwise stated. The quantity of $Fe(CN)_6^{3-}$ formed during the oxygen evolution was determined iodometrically and the quantity of $Fe(CN)_6^{4-}$ formed during the hydrogen evolution was obtained by titration with Ce^{4+}[12].

The rate of mass transfer was determined for series of experiments in sequence of decreasing current density at constant solution-flow velocity or increasing solution-flow velocity at constant current density.

The following procedure was usually applied. Before each series of experiments the working electrode was polarized in the supporting electrolyte for 60 min at the highest current density of the projected series of experiments, unless otherwise stated. After this pre-electrolysis and, without current switch-off, a calculated quantity of solution containing 1 M KOH and 1 M $K_3Fe(CN)_6$ or 1 M $K_4Fe(CN)_6$ was added to the working-electrode compartment to obtain a $K_3Fe(CN)_6$ concentration of 0.05 M.

As soon as the solution was homogeneous, a 25 cm^3 sample of solution was taken and analysed. After a polarization time of 20 min the next projected current in the series of experiments was adjusted and a 25 cm^3 sample was taken again. The same procedure was applied for the subsequent currents in the series of experiments. No current interruption occurred during the whole series of experiments. The series of experiments with various solution-flow velocities were carried out analogously.

The maximum decrease in $K_4Fe(CN)_6$ or $K_3Fe(CN)_6$ concentration for an experiment in a series was about 6%. Moreover, during a series of experiments, the volume of the solution in the working-electrode compartment became smaller because of sample taking. Both effects were corrected for.

3. RESULTS

3.1. *Parameters characterizing the behaviour of detached bubbles*

In order to characterize the bubble behaviour, the following parameters have been determined from pictures with n bubbles of a certain region just above the top of the working electrode:

$R_{d,i}$: radius of bubble i

R_d : bubble radius; $R_d = \sum_{i=1}^{n} R_{d,i}/n$

A_d : bubble cross-section; $A_d = \sum_{i=1}^{n} \pi R_{d,i}^2/n$

V_d : bubble volume; $V_d = \sum_{i=1}^{n} 4/3\pi R_{d,i}^3/n$

$R_{d,m}$: maximum of $R_{d,i}$

$R_{S,d}$: Sauter bubble radius; $R_{S,d} = 3V_d/4A_d$.

3.1.1. *Oxygen bubbles.* The Sauter bubble radius is shown as a function of current density i_O at various bulk-solution-flow velocities in Fig. 3 for the photographic method and in Fig. 4 for the high-speed moving film method. Both optical methods give practically the same results. The slight differences in $R_{S,d}$ are not caused by the difference in experimental technique but by a difference in nature of the electrode surface for the series of experiments. It is well known that, in particular, nucleation properties of an electrode surface are very sensitive to pre-treatment or history of that surface.

In Fig. 3 only two curves have been drawn; one for the results at $v_s = 0.12\,\mathrm{m\,s^{-1}}$ and the other for those at the other three solution flow velocities. Because of the small number of experimental results and the slight differences for the four solution-flow velocities, only one curve has been drawn in Fig. 4. Figures 3 and 4 show that $\log R_{S,d}$ increases linearly with increasing $\log i_O$ up to about $i_O = 2\mathrm{kA\,m^{-2}}$ and more slowly at higher current densities i_O. The slope $h_{R,S}$ of the $\log R_{S,d}/\log i_O$ curve is 0.41 at $v_s = 0.12\,\mathrm{m\,s^{-1}}$ and 0.37 at lower solution-flow velocities.

It has been found that the $\log R_d/\log i_O$, $\log R_{d,m}/\log i_O$, $\log A_d/\log i_O$ and $\log V_d/\log i_O$ curves are linear. Their respective slopes $h_R, h_{R,m}, h_A$ and h_V are independent of the bulk solution flow velocity v_s. For the photographic method the following relations for R_d, $R_{d,m}$, A_d and V_d at $v_s = 0.12\,\mathrm{m\,s^{-1}}$ have been obtained:

$$R_d = 2.6\times10^{-5} i_O^{0.44}\,\mathrm{m},\quad R_{d,m} = 22\times10^{-5} i_O^{0.28}\,\mathrm{m},$$
$$A_d = 2.4\times10^{-9} i_O^{0.85}\,\mathrm{m^2}$$
$$\text{and } V_d = 1.2\times10^{-13} i_O^{1.21}\,\mathrm{m^3},$$

where i is given in $\mathrm{kA\,m^{-2}}$. The estimate inaccuracy of the exponents of i is about 5%.

High-speed films showed that at $v_s = 0.12\,\mathrm{m\,s^{-1}}$ the bubble velocity v_b increases from 0.045 to $0.075\,\mathrm{m\,s^{-1}}$ at an increase in current density from 0.1 to $10\,\mathrm{kA\,m^{-2}}$. At $v_s = 0.04\,\mathrm{m\,s^{-1}}$ the bubble velocity v_b was higher than v_s at i_O from 1 to $10\,\mathrm{kA\,m^{-2}}$ and lower at $i_O = 0.1\,\mathrm{kA\,m^{-2}}$. Moreover, it has been found that at a constant current density and bulk solution flow, the bubble velocity is almost independent of bubble size, despite a large difference in bubble size. The diameter of the detached bubbles lies between 50 and 120 μm at $i_O = 10\,\mathrm{kA\,m^{-2}}$ and $v_s = 0.12\,\mathrm{m\,s^{-1}}$.

3.1.2. *Hydrogen bubbles.* Pictures of detached hydrogen bubbles were made for only one optical technique, *viz* the high-speed film method and for only one bulk-solution-flow velocity, *viz* $0.12\,\mathrm{m\,s^{-1}}$.

The Sauter bubble radius is plotted as a function of current density i_H, on double logarithmic scale in Fig. 5. This figure shows that $R_{S,d}$ increases at a decreasing rate with increasing current density. In the current density range from 0.1 to $1\,\mathrm{kA\,m^2}$, the experimental results can also be described by a straight line with a slope $h_{R,S}$ of about 0.25. It has also been found that $\log R_d$, $\log R_{d,m}$, $\log A_d$ and $\log V_d$ increase linearly with increasing $\log i_H$. The slopes h_R, $h_{R,m}$, h_A and h_V are, respectively, 0.27, 0.25, 0.61 and 0.97. The estimate inaccuracy of these slopes is about 5%. The parameters R_d, $R_{d,m}$, A_d and V_d are given by the following relations: $R_d = 2.9\times10^{-5} i_H^{0.27}\,\mathrm{m}$, $R_{d,m} = 7.5\times10^{-5} i_H^{0.25}\,\mathrm{m}$, $A_d = 4.5\times10^{-9} i_H^{0.61}\,\mathrm{m^2}$ and $V_d = 3.0\times10^{-13} i_H^{0.97}\,\mathrm{m^3}$ were i_H is given in $\mathrm{kA\,m^{-2}}$.

3.2. *Efficiency of gas evolution*

The volumetric rate $v_{g,b}$ of gas evolution has been determined from high-speed films. The efficiency of gas evolution $\eta_g = 100 v_{g,b}/v_g^0$ is calculated. From this rate and the theoretical one, *viz* $v_g^0 = nFi_g V_M$ where V_M is

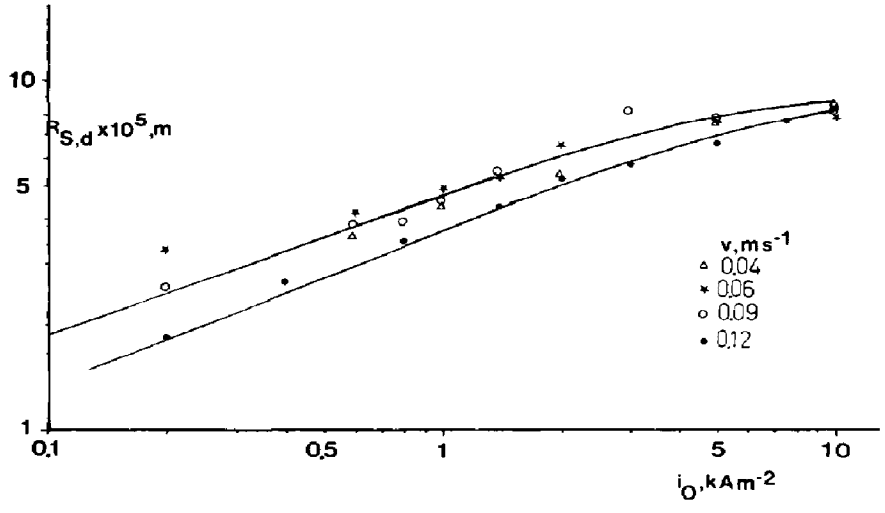

Fig. 3. Sauter bubble radius, determined by the photographic method, as a function of current density for oxygen evolution on a nickel electrode in 1 M KOH and at 298 K and various bulk-solution-flow velocites v_s.

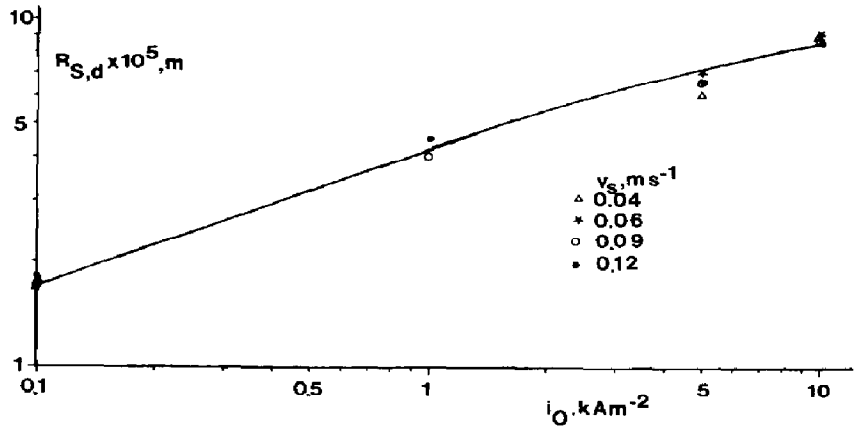

Fig. 4. Sauter bubble radius, determined by the high speed film method, as a function of current density for oxygen evolution on a nickel electrode in 1 M KOH and at 298 K and various bulk-solution-flow velocities v_s

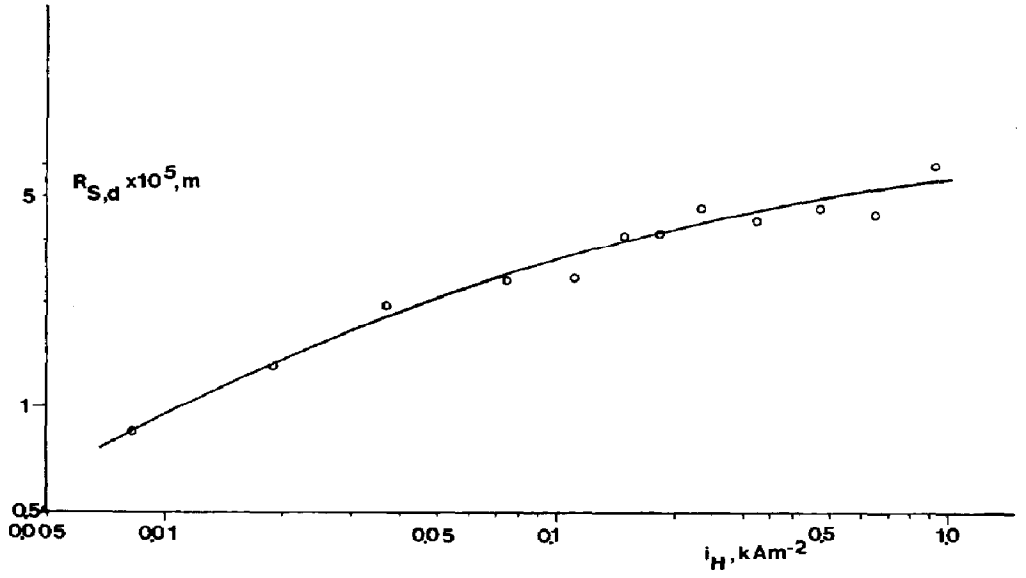

Fig. 5. Sauter bubble radius, determined by the high speed film method, as a function of current density for hydrogen evolution on a nickel electrode in 1 M KOH and at 298 K and at a bulk-solution-flow velocity of 0.12 m s^{-1}.

the volume of 1 mol gas ($V_M = 24.4 \times 10^{-3}$ m^3 mol^{-1} at 298 K).

In Fig. 6 η_g has been given as a function of current density i_O at various velocities of bulk-solution flow. The results of Fig. 6 are remarkable; only about half of the oxygen formed is evolved in the form of bubbles and the other part is transported in the dissolved state from the electrode surface.

Figure 7 shows the efficiency of gas evolution as a function of current density i_H at $v_s = 0.12$ m s^{-1}. Taking experimental inaccuracy into account, it is likely that η_g is practically constant, *ie* 75%, in the current density range from 0.05 to 1.0 kA m^{-2}. Figures 6 and 7 show that η_g for hydrogen is clearly higher than η_g for oxygen.

3.3. *Mass transfer coefficient*

The redox couple $Fe(CN)_6^{3-}/Fe(CN)_6^{4-}$ is very useful in determining the mass transfer coefficient k_i for the hydrogen-evolving electrode at $i_H > \simeq 0$ mA cm^{-2} as well as for the oxygen-evolving electrode at $i_O > \simeq 10$ mA cm^{-2}[13], since under these conditions the concentration of the indicator ion at the surface of the gas-evolving electrode is practically zero.

In this case, the mass transfer coefficient k_i of indicator ion i to a gas-evolving electrode is calculated with the well known equation

$$k_i = m_i / A_e c_i,$$

where m_i is the rate of oxidation or reduction of

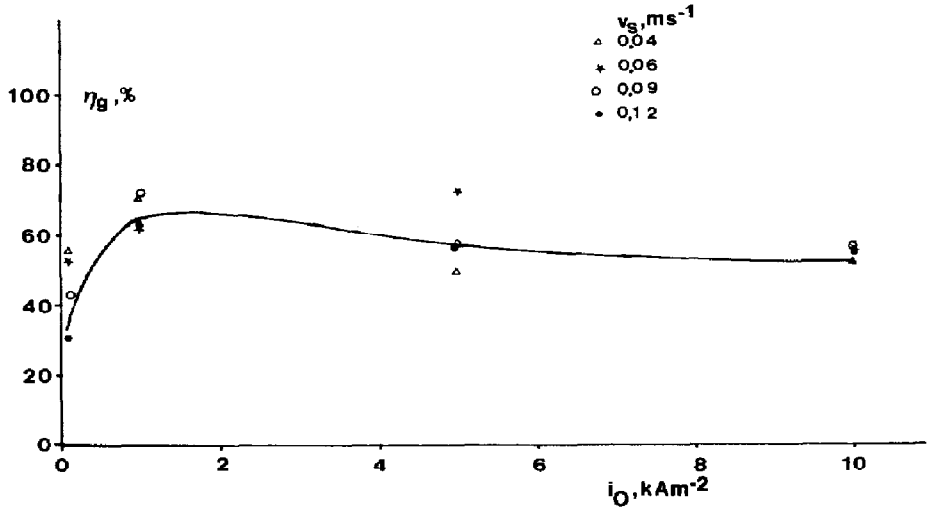

Fig. 6. Efficiency of gas bubble evolution as a function of i_O for oxygen evolution on a nickel electrode in 1 M KOH and at 298 K and various bulk-solution-flow velocities v_s.

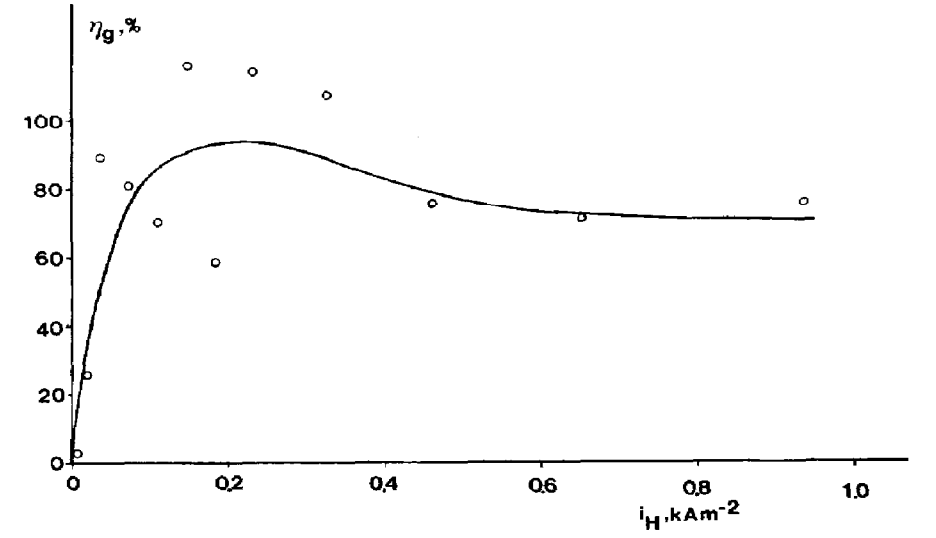

Fig. 7. Efficiency of gas bubble evolution as a function of current density for hydrogen evolution on a nickel electrode in 1 M KOH and at 298 K and a bulk-solution-flow velocity of 0.12 m s^{-1}.

indicator ions, A_e is the electrode surface area and c_i is the concentration of the indicator ion in the bulk of the solution.

In the calculation of k_i, the average concentration of the indicator ion during the experiment was used.

The current for formation of oxygen or hydrogen i_O or $i_H = i - i_i$ where i is the adjusted current density and i_i is the current density for the oxidation or reduction of indicator ions. The current density $i_i = nFm_i$.

3.3.1. *Oxygen-evolving electrode.* To determine the dependence of k_{fo} on i_O, mass transfer experiments were also carried out up to about 10 kA m^{-2}. It has been found that $k_{fo} = k_{e,fo} + P_O i^{0.85}$ for v_s from 0.04 to 0.12 m s^{-1} and $k_{e,fo}$ is higher than $k_{f,fo}$, where $k_{f,fo}$ is the mass transfer coefficient for $Fe(CN)_6^{4-}$ at forced convection and without gas evolution. Moreover, p_O decreases with increasing v_s. The mass transfer coefficient k_{fo} is given in Fig. 8 as a function of $i_O^{0.85}$ for an oxygen-evolving nickel electrode in 1 M KOH as supporting electrolyte, at 298 K and various v_s. The results at $i_O = 0$ kA m^{-2} were obtained from experiments by measuring the current of $Fe(CN)_6^{3-}$ reduction at a potential of 450 mV *vs sce*. At this potential the limiting current for oxidation of $Fe(CN)_6^{4-}$ was obtained.

Linear extrapolation of a $k_{fo}/i_O^{0.85}$ curve gives k_{fo} at

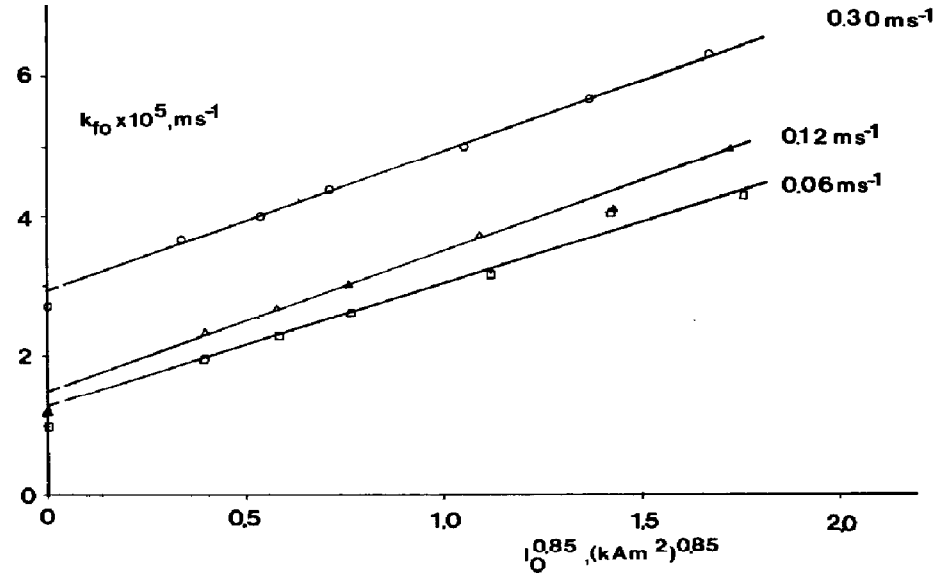

Fig. 8. Mass transfer coefficient for $Fe(CN)_6^{4-}$ to an oxygen-evolving nickel electrode in 1 M KOH and at 298 K and three different bulk-solution velocities is plotted *vs* the current density of oxygen evolution.

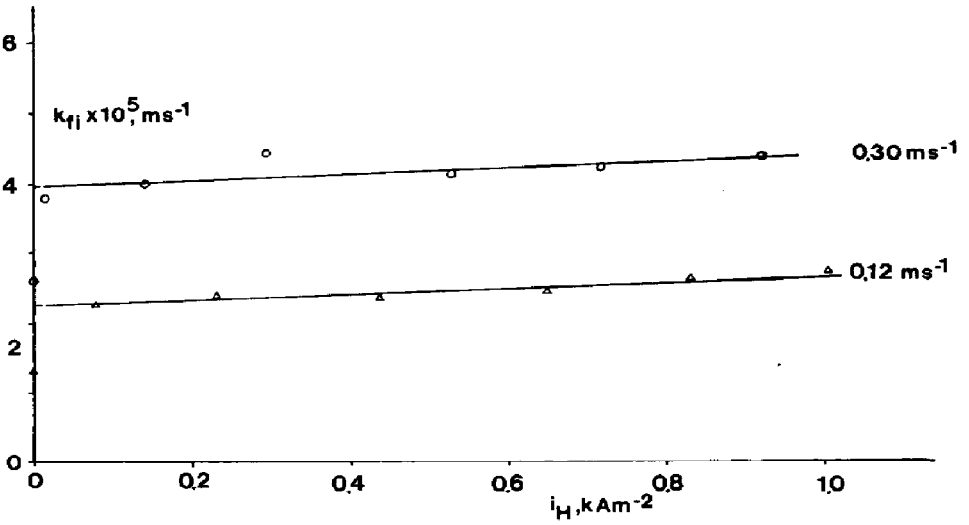

Fig. 9. Mass transfer coefficient for $Fe(CN)_6^{3-}$ to a hydrogen-evolving nickel electrode in 1 M KOH and at 298 K and two different bulk-solution flow velocities v_s is plotted *vs* the current density of hydrogen evolution.

$i_O = 0\,kA\,m^{-2}$, denoted by $k_{e,fo}$. Figure 8 shows that $k_{e,fo}$ is larger than $k_{f,fo}$.

3.3.2. *Hydrogen-evolving electrode.* Figure 9 shows the mass transfer coefficient k_{fi} as a function of i_H for a hydrogen-evolving electrode in 1 M KOH as supporting electrolyte, at 298 K and two different flow velocities. The mass transfer coefficient $k_{f,fi}$ was determined by measuring the current at a working electrode potential of -0.5 V. From Fig. 9 it follows that the slight increase in k_{fi} is proportional to i_H. Linear extrapolation of the straight lines of Fig. 9 gives $k_{e,fi}$. Figure 9 shows that both velocities of solution flow $k_{e,fi}$ are clearly higher than $k_{f,fi}$. To check the relation between k_{fi} and i_H, represented in Fig. 9, mass transfer experiments were also carried out at up to i_H is about $10\,kA\,m^{-2}$. It has been found that $k_{fi} = k_{e,fi} + p_H i_H$ and p_H decreases with increasing i_H.

4. THEORY

The rate of mass transfer of indicator ions to a gas-evolving electrode is described by a new model. In this model only the detaching bubbles are taken into consideration. This means that the adhered bubbles have no influence upon the rate of mass transfer.

The formation, growth and detachment of a bubble on a site of the electrode surface require a time t_d. On the same site this phenomenon is constantly repeated. When bubble departs from a site on the electrode surface, it is assumed that an electrode surface area of $a_d A_d$ comes into contact with fresh bulk electrolyte having the bulk concentration of indicator ions, c_i, where A_d is the cross-section of a detached bubble and a_d is a constant factor.

To calculate the mass transfer coefficient the following additional simplifications are still made:

—the radius, the cross-section and the volume of all detached bubbles are constant and, respectively, R_d, A_d and V_d;
—the distribution of the bubble-depart sites across the electrode surface is uniform;
—the bubble cycle time t_d is equal for all electrode sites;
—the detaching and rising bubbles induce no solution flow except the flow necessary for refreshment of solution at the electrode surface.

From the rate of volumetric gas bubble formation per unit surface area, $v_{g,b}$, and the volume V_d of a detached bubble it follows that the number of detached bubbles per unit surface area and time

$$N = v_{g,b}/V_d. \tag{1}$$

Since the density of sites from which bubbles depart, $d = Nt_d$, the fraction of electrode surface coming into contact with fresh bulk electrolyte in period t_d is given by

$$s = Nt_d a_d A_d. \tag{2}$$

In the absence of migration and convection, the mass transfer coefficient for indicator ions can be obtained by so-called semi-infinite linear diffusion at a plane electrode.

The mass transfer coefficient for indicators, k_i, can be derived from the well known relation for the rate of mass transfer. It can be shown that

$$k_i = D_i^{1/2}/\pi^{1/2}t^{1/2}, \tag{3}$$

where t is the time passed after detachment of a bubble. At $t = 0$ the concentration of indicator ions does not depend on the distance from the electrode surface.

For the fractions of the electrode surface coming into contact with fresh bulk electrolyte after detachment of bubbles, the average mass transfer coefficient for indicator ions, $k'_{i,a}$ in the period t_d is

$$k'_{i,a} = \frac{1}{t_d}\int_0^{t_d} k_i \,\mathrm{d}t. \tag{4}$$

After introduction of Equation (3) into Equation (4) and after integration of the resulting integral it is found that

$$k'_{i,a} = 2D_i^{1/2}/\pi^{1/2}t_d^{1/2}. \tag{5}$$

Since in a convectionless solution the mass transfer coefficient for the uncovered fraction $1-s$ of the electrode surface not coming into contact with fresh solution is zero, the total mass transfer coefficient k_i^0 for a gas-evolving electrode in a convectionless soluton

$$k_i^0 = k'_{i,a}s. \tag{6}$$

From Equations (1), (2) and (6) it follows that

$$k_i^0 = 2a_d A_d v_{g,b} D_i^{1/2} t_d^{1/2}/\pi^{1/2} V_d. \tag{7}$$

From relations (1), (2) and (7) it can be shown that

$$k_i^0 = 2a_d A_d D_i^{1/2} v_{g,b}^{1/2} d^{1/2}/\pi^{1/2} V_d^{1/2}. \tag{8}$$

The mass transfer coefficient for indicator ions to a gas-evolving electrode in a convectionless solution is described by Equations (7) as well as by Equation (8).

The effect of forced convection on mass transfer coefficient is discussed in the next section.

For a bubble-free electrode surface under forced convection the mass transfer coefficient is given by k_f. Consequently, for the fraction $1-s$ of the electrode surface not in contact with fresh bulk electrolyte the mass transfer coefficient is equal to k_f.

For the fraction s of electrode surface in contact with fresh bulk solution, the calculation of the average mass transfer coefficient is complicated. During the bubble cycle the mass transfer coefficient is greater than k_f directly after bubble detachment and becomes equal to k_f after a certain time t_1.

The solution in the diffusion layer is regarded as a convectionless solution.

The mass transfer coefficient, directly after bubble detachment, is equal to k'_i. Since k'_f at t_1 is equal to k_f, it can be shown that

$$t_1 = D_i/\pi k_f^2. \tag{9}$$

The bubble cycle time t_d is divided into two parts, *viz* t_1 and $t_d - t_1$.

For the fraction s of the electrode surface and assuming the bubble cycle time is greater than t_1, the mass transfer coefficient during time $t_d - t_1$ is given by k_f and the average one during time t_1 by

$$k'_{f,i,a} = \frac{1}{t_1}\int_0^{t_1} k'_i \,\mathrm{d}t. \tag{10}$$

By substitution of k'_i by Equation (3) into Equation (10) and after integration it follows that

$$k'_{f,i,a} = 2D_i^{1/2}/\pi^{1/2}t_1^{1/2}. \tag{11}$$

The mass transfer coefficient averaged over one bubble cycle

$$k'_{f,i,a^*} = \frac{k'_{f,i,a}t_1 + k_f(t_d - t_1)}{t_d}. \tag{12}$$

From Equations (9), (11) and (12) it is found that

$$k'_{f,i,a^*} = k_f + \frac{D_i}{\pi k_f t_d}. \tag{13}$$

The total mass transfer coefficient for a gas-evolving electrode under forced convection is

$$k_i = k_f(1-s) + k'_{f,i,a^*}s. \tag{14}$$

From Equations (13) and (14) it follows that

$$k_i = k_f + \frac{D_i s}{\pi k_f t_d} \tag{15}$$

and from Equations (1), (2) and (14) that

$$k_i = k_f + \frac{D_i a_d A_d v_{g,b}}{\pi k_f V_d}. \quad (16)$$

The first term of Equation (16) incorporates the mass transfer at forced convection and in the absence of gas bubble formation; the second term gives the contribution caused by detached bubbles.

In the next discussion, it is assumed that $t_1 > t_d$. Since, in this case $k'_{f,i,a^*} = k'_{f,i,a}$, the mass transfer coefficient k_i is given by

$$k_i = k_{f,i}(1 - s) + k'_{f,i,a}s. \quad (17)$$

When the first term of Equation (17) is much smaller than the second one, then

$$k_i = k'_{f,i,a}. \quad (18)$$

From Equations (1), (2), (11) and (18) and substituting t_1 of Equation (11) by t_d it follows that

$$k_i = \frac{2a_d A_d D_i^{1/2} v_{g,b}^{1/2} d^{1/2}}{\pi^{1/2} V_d^{1/2}}. \quad (19)$$

Comparing Equations (19) and (8) shows that, in this case, the relations for k_i and k_i^0 are equal.

5. DISCUSSION

5.1. *Behaviour of detached bubbles*

The size of a bubble at the moment of departure from the electrode surface is less than that of rising bubbles when coalescence of detached bubbles occurs. Coalescence of detached bubbles is affected by various factors, *eg* bubble density, solution flow velocity, length of bubble trajectory in the electrolytic cell and the nature of gas and solution. The literature on electrochemically formed gas bubbles has been recently reviewed by Vogt[14].

Results on the behaviour of oxygen as well as hydrogen bubbles formed during electrolysis at forced convection have already been published[10, 15, 16].

The average radii for oxygen as well as hydrogen detached bubbles are proportional to, respectively, $i_O^{0.44}$ and $i_H^{0.27}$ (Sections 3.1.1. and 31.2). Both dependences are clearly greater than those found by Bongenaar *et al.*[15]. They determined the radius of bubbles at the outlet of an electrolysis cell with a 50-cm-high working electrode in 30 wt% KOH at a temperature of 353 K and solution flow velocity of 0.5 m s^{-1}.

The experimental conditions in this investigation, however, deviate strongly from those used in[15, 16], so that only a qualitative agreement might be expected.

Since bubbles present in the solution just above the top of the working electrode were pictured, and also the low height of the working electrode, *viz* 5.45 mm, it is likely that coalescence of bubbles rising in the solution will not have a significant effect on experimental bubble size.

The oxygen bubbles, formed by coalescence of bubbles which had adhered to the electrode surface, jumped perpendicularly from the electrode surface[4].

The density of rising oxygen bubbles in the solution near the electrode surface is relatively low, since no layer of free oxygen bubbles glides over the layer of attached oxygen bubbles[16]. At the hydrogen-evolving electrode bubbles glide over the layer of attached hydrogen bubbles. It is well known, that in alkaline solution, hydrogen bubbles do not coalesce as easily as oxygen bubbles do. Consequently, the bubble size determined in this investigation is almost equal to that for the bubbles departing from the electrode surface. Obviously, coalescence of attached bubbles can affect the experimental results strongly.

5.2. *Efficiency of gas evolution*

The efficiency of gas evolution is much higher for the hydrogen-evolving electrode than for the oxygen-evolving electrode (Figs 6 and 7). The calculated efficiency of gas evolution given in[9] is very much less than the experimental results given in Fig. 7. Additional experiments are necessary to obtain more accurate results.

It is likely that the efficiency of gas evolution determined from pictures just above the top of the working electrode, is less than that for the working electrode because of gas absorption by bubbles rising from the supersaturated solution near the gas-evolving electrode. Assuming a negligible difference in both efficiencies, the supersaturation of gas at the gas-evolving electrode can be calculated when the mass transfer coefficient for the dissolved gas is well known. Assuming that k for the gas-evolving cylindrical electrode used in measuring the efficiency of gas evolution is equal to the gas-evolving flat-plate electrode then, using $D_H = 3.0 \times 10^{-9}$ m^2 s^{-1}[17], $D_O = 1.59 \times 10^{-9}$ m^2 s^{-1}[18], $D_{fi} = 7.9 \times 10^{-10}$ m^2 s^{-1}, $D_{fo} = 7.0 \times 10^{-10}$ m^2 s^{-1}[11] and the relations $k_H = (D_H/D_{fi})^{1/2} k_{fi}$ and $k_O = (D_O/D_{fo})^{1/2} k_{fo}$, it can be calculated that the hydrogen supersaturation of the solution at a hydrogen-evolving electrode in 1 M KOH and at 1 kA m^{-2} and $v_s = 0.12$ m s^{-1} is equal to 25 mM and the oxygen supersaturation of the solution at an oxygen-evolving electrode in 1 M KOH and at 1 kA m^{-2} and $v_s = 0.12$ m s^{-1} is 23 mM. This result agrees very well with that obtained with a rotating ring–cone electrode[19].

5.3. *Mass transfer at gas-evolving electrode*

Gas bubble evolution at an electrode causes solution flow near the electrode surface. For a hydrogen-evolving electrode in alkaline solution, the hydrodynamic model was proposed to describe the mass transfer of indicator ions[5]. In this model, the effect of the solution flow induced by bubbles is taken into account exclusively. It is likely that this effect is reduced at increasing velocity of forced solution flow.

Gas bubbles formed at an electrode block the current passage for a part of the electrode surface during their attachment and impede the mass transfer of indicator ions to the electrode surface. After detachment, the space which had been occupied by the detached bubbles is filled up with solution. In the coalescence model used to describe the mass transfer of indicator ions to an oxygen-evolving electrode in alkaline solution[4], it is assumed that this solution has the composition of bulk solution. The solution flow needed to fill up the space occupied by detached bubbles is considered as a solution flow, the velocity of

which has no direct effect on the rate of mass transfer.

The bubble density d has to be used to calculate t_d. Unfortunately, this factor is unknown. For the sake of reliability it is assumed that $t_1 < t_d$ if $k < 3k_e$, in the case that $k_e = k$ in the absence of bubble formation and has been obtained by extrapolation of the k/i curve. Consequently, relation (16) is only used at relatively low values of k, *viz* $k < 3k_e$.

It is assumed in the following sections that the experimental results obtained for the wire electrode can be used to elucidate the mass transfer measurements for the rectangular plate electrode.

5.3.1. *Oxygen-evolving electrode.* From Figs 4 and 6, the factor $D_{fo}A_d v_{g,b}/\pi V_d$ at $v_s = 0.12\,\mathrm{m\,s^{-1}}$ and at various i_O can be determined when it is taken into consideration that $R_{S,d} = 3V_d/4A_d$, $v_{g,b} = \eta_g v_g^0$ and $v_g^0 = i_O V_M/4F$.

Since $V_M = 24.5 \times 10^{-3}\,\mathrm{m^3\,mol^{-1}}$ it follows that at 298 K $v_g^0 = 0.634 \times 10^{-4} i_O\,\mathrm{m\,s^{-1}}$ where i_O is given in $\mathrm{kA\,m^{-2}}$.

It has been found that, for the oxygen-evolving electrode at $v_s = 0.06$ and $0.12\,\mathrm{m\,s^{-1}}$, $k_{e,fo}$ is higher than $k_{f,fo}$. This means that the effect of the hydrodynamic convection of solution which occurs at very low current densities, *viz* $< 0.05\,\mathrm{kA\,m^{-2}}$, has to be taken into account. To verify the proposed model, $k_{e,fo}$ has to be used.

For an oxygen-evolving electrode the factor $(k_{fo} - k_{e,fo})k_{e,fo}$ is plotted *vs* $D_{fo}A_d v_{g,b}/\pi V_d$ in Fig. 10. The experimental results are scattered around a straight line with a slope $a_{d,O}$ of 1.7. This means that the refreshment mechanism is very effective in enhancing the mass transfer of indicator ions to the surface of an oxygen-evolving electrode.

For the oxygen-evolving electrode, the hydrodynamic mechanism is of still less importance in this case, because of the behaviour of detaching oxygen bubbles. These bubbles jump perpendicularly from the electrode surface and cause only a weak vertical hydrodynamic flow of solution near the electrode surface. The detached rising oxygen bubbles do not form a curtain near the electrode surface as the detached rising hydrogen bubbles do.

Assuming $t_1 > t_d$ at $i_O > 1\,\mathrm{kA\,m^{-2}}$, the mass transfer coefficient is then given by Equation (19). From Equation (19) it can be deduced that $d = V_d k_{fo}^2/4a_d^2 A_d^2 D_{fo} v_{g,b}$. The bubble density d is calculated at various i_O and at $v_s = 0.12\,\mathrm{m\,s^{-1}}$.

Using the mass transfer coefficient k_{fo}, *viz* 14×10^{-5}, 9.5×10^{-5} and $3.6 \times 10^{-5}\,\mathrm{m\,s^{-1}}$ for, respectively $i_O = 10$, 5 and $1\,\mathrm{kA\,m^{-2}}$, $D_{fo} = 7.0 \times 10^{-10}\,\mathrm{m^2\,s^{-1}}$[11], $a_{d,O} = 1.7$ (Section 5.3.1), $v_{g,b} = 0.634 \times 10^{-4} f_g i_O\,\mathrm{m\,s^{-1}}$, $A_d = 2.4 \times 10^{-9} i_O^{0.85}\,\mathrm{m^2}$ (Section 3.14) and $V_d = 1.2 \times 10^{-13} i_O^{1.21}\,\mathrm{m^3}$ where i_O is given in $\mathrm{kA\,m^{-2}}$ it was calculated that $d_O = 1.18 \times 10^8$, 1.58×10^8 and $2.60 \times 10^8\,\mathrm{m^{-2}}$ for, respectively $i_O = 10$, 5 and $1\,\mathrm{kA\,m^{-2}}$. In this case, d_O is proportional to $i_O^{-0.34}$.

When d is taken as A_d^{-1}, it can be shown that in that case $d_O = 0.59 \times 10^8$, 1.06×10^8 and $4.16 \times 10^8\,\mathrm{m^{-2}}$ for, respectively $i_O = 10$, 5 and that $1\,\mathrm{kA\,m^{-2}}$ and d_O is proportional to $i_O^{-0.9}$. Comparing both series of d_O, it follows that the order of their magnitude is the same but that their dependence on i_O differs strongly.

The density of bubbles present on the electrode surface is proportional to about $i_O^{0.9}$[10]. In particular, it was found that an increasing number of attached bubbles are small ones.

A great part of these small bubbles coalesce without forming detached bubbles. Consequently, it is likely that these small bubbles can be left out of consideration in describing the mass transfer of indicator ions to a gas-evolving electrode.

From the preceding discussion it can be concluded that the new model can describe the mass transfer of indicator ions to an oxygen-evolving electrode at forced as well as at natural convection. In the latter case, some effect of hydrodynamic flow of solution will also occur at low current densities.

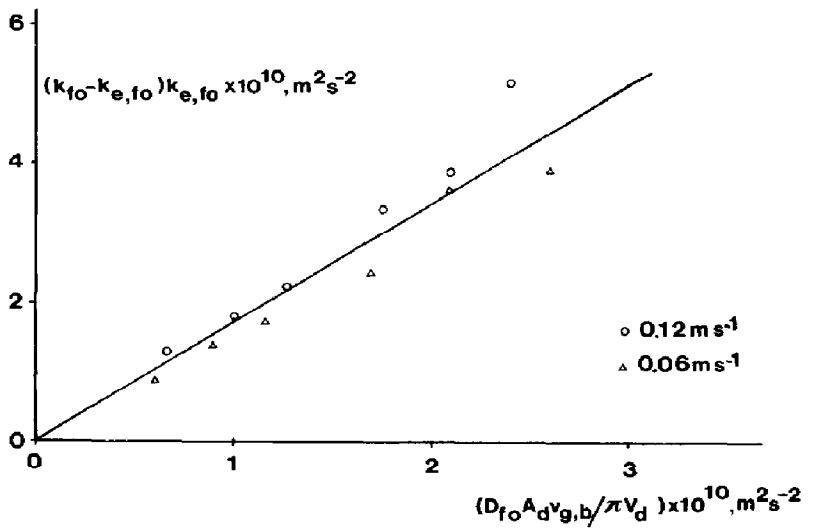

Fig. 10. The factor $(k_{fo} - k_{e,fo})k_{e,fo}$ is plotted *vs* $D_{fo}A_d v_{g,b}/\pi V_d$ for an oxygen-evolving nickel electrode in 1 M KOH and at 298 K and two different bulk-solution-flow velocities.

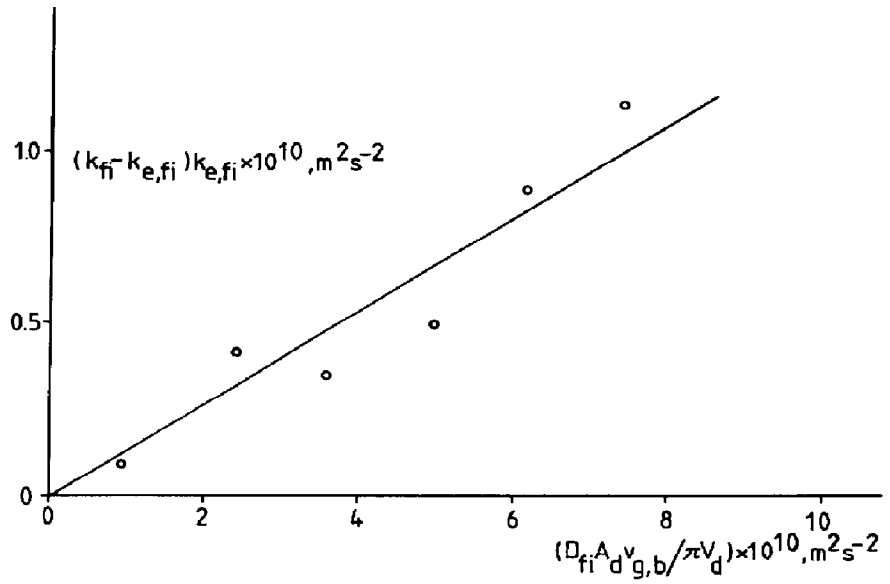

Fig. 11. The factor $(k_{fi}-k_{e,fi})k_{e,fi}$ is plotted *vs* $D_{fi}A_d v_{g,b}/\pi V_d$ for a hydrogen-evolving nickel electrode in 1 M KOH and at 298 K and a bulk-solution-flow velocity of 0.12 m s^{-1}.

5.3.2. *Hydrogen-evolving electrode.* From the k_{fi}/i_H curves and $k_{f,fi}$ at various v_s, it follows that in the range of very low i_H, *viz* < 0.02 kA m^{-2}, k_{fi} increases from $k_{f,fi}$ at current densities i_H where no bubble formation takes place, to a much higher value than $k_{f,fi}$ at $i_H > 0.02$ kA m^{-2}. The increase of k_{fi} with increasing i_H is much lower and is proportional to i_H (Fig. 9). This increment is caused either by a stronger flow of solution near the electrode surface or an increasing effect of solution refreshment at the electrode surface or by both.

In the following discussion, it is assumed that it is only this refreshment mechanism that determines the increment of k_{fi}.

In the range of current densities i_H where $k_{fi} < 3k_{e,fi}$, it is assumed, in the case of the oxygen-evolving electrode, that the rate of mass transfer coefficient for the hydrogen-evolving electrode is given by Equation (16).

For hydrogen-evolving electrodes it has been found that $k_{e,fi}$ is clearly higher than $k_{f,fi}$ in the investigated range of solution flow velocities. This result can be explained by the formation of a curtain of rising bubbles near the electrode surface and by slipping bubbles attached to the electrode surface.

In the range of very low current densities both phenomena cause a hydrodynamic flow of the solution enhancing the mass transfer near the electrode surface.

To elucidate the contribution of the refreshment mechanism to mass transfer, it is preferred to use k_e instead of k_f.

In Fig. 11 the difference $k_{fi}k_{e,fi}-k_{e,fi}^2$ (Fig. 9) is plotted *vs* $D_{fi}A_d v_{g,b}/\pi V_d$ (Figs 5 and 7) for a hydrogen-evolving electrode at $v_s = 0.12$ m s^{-1}, where $R_{S,d} = 3V_d/4A_d$, $v_{g,b} = \eta_g v_g^0$ and v_g^0 at 298 K is 1.268×10^{-4} i_H m s^{-1} where i_H is given in kA m^{-2}. The slope of the straight line drawn in Fig. 11 is equal to $a_{d,H} = 0.14$. This value of $a_{d,H}$ is low and indicates low effectiveness of the refreshment mechanism for the hydrogen-evolving electrode. If the hydrodynamic mechanism also contributes to the increment of the mass transfer coefficient at $v_s = 0.12$ m s^{-1}, the factor $a_{d,H}$ has then to be smaller than 0.14. In this case, the effectiveness of the refreshment mechanism becomes still lower.

REFERENCES

1. H. Vogt, *Comprehensive Treatise of Electrochemistry* (Edited by E. Yeager, J. O'M. Bockris, B. E. Conway and S. Sarangapani), Vol. 6, p. 445 (1983).
2. N. Ibl, E. Adam, J. Venczel and E. Schalch, *Chem. Ing. Tech.* **43**, 202 (1971).
3. K. Stephan and H. Vogt, *Electrochim. Acta* **24**, 11 (1979).
4. L. J. J. Janssen and S. J. D. van Stralen, *Electrochim. Acta* **26**, 1011 (1981).
5. L. J. J. Janssen and E. Barendrecht, *Electrochim. Acta* **24**, 693 (1979).
6. I. Rousar and V. Cezner, *Electrochim. Acta* **20**, 289 (1975).
7. T. R. Beck, *J. electrochem. Soc.* **116**, 1038 (1969).
8. H. Vogt, *Electrochim. Acta* **23**, 205 (1978).
9. H. Vogt, Extended Abstracts 34th meeting ISE, Erlangen, 0413 (1983).
10. C. W. M. P. Sillen, Thesis, Eindhoven University of Technology (1983).
11. L. J. J. Janssen, *Electrochim. Acta* **23**, 81 (1978).
12. J. M. Kolthoff and E. B. Sandell, *Textbook of Quantitative Inorganic Analysis*. Macmillan, New York (1952).
13. L. J. J. Janssen and J. G. Hoogland, *Electrochim. Acta* **18**, 543 (1973).
14. H. Vogt, *Fortschritte der Verfahrenstechnik* **20**, 369 (1982).
15. B. E. Bongenaar-Schlenter, L. J. M. Konings, C. J. Smeyers, J. H. G. Verbunt, E. Barendrecht, L. J. J. Janssen, W. M. Sluijter and S. J. D. van Stralen,

Hydrogen as an energy carrier, *Proc. 3rd Int. Seminar*, Lyon 25–27 May 1983, p. 206. D. Reidel, Dordrecht (1983).
16. L. J. J. Janssen, C. W. M. P. Sillen, E. Barendrecht and S. J. D. van Stralen, *Electrochem. Acta* **29**, 633 (1984).
17. A. M. Yatkovski and N. A. Fedotov, *R. J. Phys. Chem.* **43**, 575 (1969).
18. F. T. B. J. van den Brink, Thesis Eindhoven (1981).
19. L. J. J. Janssen and E. Barendrecht, *Electrochim. Acta* **29**, 1207 (1984).